



Generalized solution of functionally graded hollow cylinder under torsional load

Y. Bayat^a, M. Alizadeh^{b,*} and A. Bayat^c

^aYoung Researchers Club, Mashhad Branch, Islamic Azad University, Mashhad, Iran

^bDepartment of Mechanical Engineering, Iran University of Science & Technology, Tehran, Iran

^cDepartment of Mechanical Engineering Isfahan University of Technology, Isfahan, Iran

Article info:

Received: 07/06/2012

Accepted: 19/11/2012

Online: 03/03/2013

Keywords:

Functionally graded material,
Hollow cylinder,
Torsion,
Finite element method,
Arbitrarily varying gradients.

Abstract

In this paper, a general solution for torsion of hollow cylinders made of functionally graded materials (FGM) was investigated. The problem was formulated in terms of Prandtl's stress and, in general, the shear stress and angle of twist were derived. Variations in the material properties such as Young's modulus and Poisson's ratio might be arbitrary functions of the radial coordinate. Various material models from the literature were also used and the corresponding shear stress and angle of twist were individually computed. Moreover, by employing ABAQUS simulations, finite element results were compared with the analytical ones.

1. Introduction

Torsion is one of the interesting fields for researches. In 1903, Prandtl [1] presented a membrane analogy for torsional analysis and proved the accuracy and efficiency of his approximation. Baron [2] studied torsion of hollow tubes by multiplying the connected cross sections. He used an iterative method to satisfy the equilibrium and compatibility equations. A computational method for calculating torsional stiffness of multi-material bars with arbitrary shape was studied by Li et al. [3]. In this work, they considered additional compatibility and equilibrium equations in common boundaries of different materials in their formulation and got good results. Mijak [4] considered a new method to design an

optimum shape in beams with torsional loading. In his work, cost function was torsional rigidity of the domain and constraint was the constant area of the cross-section while shape parameters were co-ordinates of the finite element nodes along the variable boundary. The problem was solved directly by optimizing the cost function with respect to the shape parameters. He solved this problem using finite elements (FE method). A method based on finite elements for torsional analysis of prismatic bars by modeling only a small slice of the bar was published by Jiang et al. [5]. Another work related to the torsion in prismatic bars was introduced by Louis et al. [6], in which they presented a solution using a power fit model for the torsion problem of a rectangular prismatic bar. Recently, Doostfateme et al. [7] obtained a closed-form

*Corresponding author

Email address: ma_alizadeh@iust.ac.ir

approximate formulation for torsional analysis of hollow tubes with straight and circular edges. In this work, the problem was formulated in terms of Prandtl's stress function. Also, accuracy of the formulas was verified by accurate finite element method solutions.

In recent years, the composition of several different materials has been often used in structural components in order to optimize responses of the structures subjected to thermal and mechanical loads. Functionally graded materials (FGMs) are suitable for achieving this purpose. Although they were first invented as a thermal shield to sustain very high temperature gradients in thin structures [8], FGMs are currently being used for many other applications such as wear-resistant linings, heat exchanger tubes, thermoelectric generators and heat-engine components. Actually, FGMs are mixtures of two or more different materials. Volume fraction of each material varies continuously along certain direction(s). The gradual change of material properties can be tailored to meet the requirements of different applications and working environments.

Many relations are available for characterizing the varying properties of functionally graded materials [9]. Horgan [10] studied the modulus of elasticity as $E(r) = E_0 r^n$ in the radial direction for investigating the impact problem in cylinder (n as the anisotropy constant $(-2 \leq n \leq 2)$). Kassir [11,12] assumed the shear modulus as a power function of the depth coordinate $\mu(y) = \mu_0 y^n$ while the Poisson's ratio was constant. Tutuncu [13] expanded the Horgan work for thick-walled FGM cylinders with exponentially-varying properties.

An analytical formulation for the torsional analysis of FG elastic bars with circular cross sections was presented by Horgan [14], in which it was supposed the shear modulus of rigidity as a function of radius. Moeini [15] studied the torsion of a FGM cylinder with FE model. An analytical formulation for the torsional analysis of functionally graded hollow tubes of arbitrary shape was carried out by Arghavan et Al. [16]. In this paper, shear

modulus of rigidity was supposed to change continuously as power-low form between two constituent phases on the inner and outer boundaries across the thickness.

In the above-mentioned works, varying material properties has been usually treated as specific gradient variation. However, in practice, material properties often vary in an arbitrary manner. For the sake of overcoming the restriction of gradient assumption of special forms, it is much desirable to present an approach for dealing with an arbitrary gradient variation. For this purpose, a new formula for the generalized twist was presented by Ecsedi [17]. This formula was valid for linearly elastic, nonhomogeneous and anisotropic beams of solid cross section. Batra [18] studied the torsion of FG circular cylindrical solid bar made of either an isotropic compressible or an isotropic incompressible linear elastic material with the material varying only in the axial direction. In another work, Tutuncu et al. [19] presented a novel approach to stress analysis of the pressurized FGM cylinders, disks and spheres. In this work, the relationships for arbitrary function of FG materials were investigated using complementary functions method. Xian-Fang et al. [20] developed an analytical solution for pressurized functionally graded hollow cylinder with arbitrarily varying material properties which was solved by expanding the solution as a series of Legendre polynomials. In addition, thermoelastic analysis of a cylindrical vessel of functionally graded materials was presented by Long Peng et al. [21], in which material properties were arbitrary functions in radial direction. Nie et al. [22] recently derived some mathematical relationships for different material tailoring for orthotropic elastic rotating disks. In this study, they investigated how to tailor material moduli for achieving a desirable stress field in a rotating disk composed of radially inhomogeneous materials.

The purpose of this study was to present analytical formulas for torsional analyses of an FG hollow cylinder with material properties of arbitrary nonhomogeneity. In fact, material properties of functionally graded material were assumed to be arbitrary functions of radial

direction. The relations of the shear stress and twist angle were generally obtained. Various material models such as power law function, exponential law and combined ceramic–metal material were used. For power and exponential law functions, the relation of shear stress and angle of twist were separately obtained. Besides, for combined ceramic-metal models, the numerical results were represented analytically using Maple calculation. Finally, by employing ABAQUS simulations, the finite element method, compared with the analytical results, was implemented to solve the problem. It should be emphasized once again that the analytical solution procedure is not confined to any particular choice of material model; it is equally suitable for arbitrary functions, defining the gradient variation of material properties.

2. Governing equations

A typical cross-section of a FGM circular hollow cylinder with the internal radius ‘a’ and external radius ‘b’, as shown in Fig. 1, was considered.

Regarding the Cartesian-coordinates, the torsion is applied in z-axis direction. The dimensionless variable $k = b / a$ is used in the derivation of the formulas. The governing equations can be expressed as the following [14]:

$$\nabla \cdot \left(\frac{1}{\mu} \nabla \phi \right) = -2\alpha \tag{1}$$

$$T = 2 \int_R \phi dR + 2\phi_1 A_{S_1} \tag{2}$$

$$\oint_{S_1} \frac{\tau}{\mu} dS = 2\alpha A_{S_1} \tag{3}$$

$$\begin{cases} \phi = 0 & \text{at } S_0 \\ \phi = \phi_1 & \text{at } S_1 \end{cases} \tag{4}$$

where T , α and A_{S_1} are torsional couple, angle of twist per unit length and area bounded by S_1 respectively. Also τ represents shear stress that can be expressed as follows:

$$\tau = -\frac{d\phi}{dr} \tag{5}$$

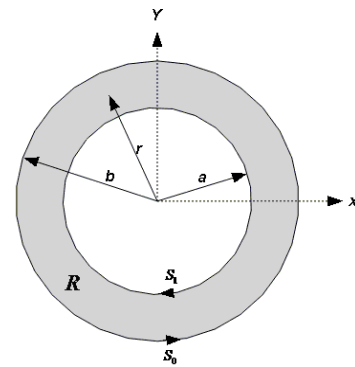


Fig. 1. Cross section of a hollow circular cylinder with internal radius “a” and external radius “b”.

where the Prandtl’s stress function ϕ must be chosen to satisfy the boundary conditions (3, 4). Eq. (1) for axisymmetric case was [23]:

$$\frac{1}{r} \left[\frac{d}{dr} \left(\frac{r}{\mu(r)} \frac{d\phi}{dr} \right) \right] = -2\alpha \tag{6}$$

As an approximation, it was assumed that the shear stress variation was in the radial direction.

The solution of Eq. (6) was:

$$\phi(r) = -\alpha \int_a^r r \mu(r) dr + c_1 \int_a^r \frac{\mu(r)}{r} dr + c_2 \tag{7}$$

where c_1 and c_2 are integration constants.

By substituting Eq. (7) in Eq. (5), the shear stress could be expressed as shown below:

$$\tau = \alpha r \mu(r) - c_1 \frac{\mu(r)}{r} \tag{8}$$

From the boundary conditions (3, 4) results:

$$\begin{cases} c_1 = 0 \\ c_2 = \alpha \int_a^b r \mu(r) dr \end{cases} \tag{9}$$

Also, the stress function ϕ and the shear stress τ could be written as:

$$\begin{cases} \phi(r) = \alpha \int_r^b r \mu(r) dr \\ \tau = \alpha r \mu(r) \end{cases} \tag{10}$$

2.1. Model A: The shear modulus used a power law function as

$$\mu = \mu_0 \left(\frac{r}{a}\right)^n \tag{11}$$

where n is the inhomogeneity constant which can be determined empirically. The range $-2 \leq n \leq 2$ was used for the inhomogeneity constant. μ_0 was the shear modulus for a homogeneous material $n = 0$ which could be clearly expressed by the Lamé's coefficient as follows:

$$\mu_0 = \frac{E_0}{2(1+\nu)} \tag{12}$$

Furthermore, the Poisson's ratio was assumed to be constant.

By substituting Eq. (11) in Eq. (10) and using Eq. (2) and (3), the torque of twist and the shear stress were obtained as:

$$T = \frac{2\pi \mu_0 a^4 (k^{n+4} - 1)}{n + 4} \alpha \quad \text{and} \quad \tau = \mu_0 \alpha \frac{r^{n+1}}{a^n} \tag{13}$$

where $k = b/a$. Use of Eq. (13) resulted in:

$$\tau = \frac{(n+4)T}{2\pi a^{n+4} (k^{n+4} - 1)} r^{n+1} \tag{14}$$

2.2. Model B: Shear modulus with exponential form

For this case, the shear modulus obeyed the following relation:

$$\mu = \mu_0 e^{-\frac{n}{a}r} \tag{15}$$

where n is the inhomogeneity constant and μ_0 is the shear modulus for a homogeneous material $n = 0$. The range of n implemented here was $-1 \leq n \leq 1$. Also, the Poisson's ratio was assumed to be constant.

From Eq. (15), the torque of twist was obtained as:

$$T = \frac{2\pi \mu_0 a^4 \alpha}{n^4} (I(n) - I(nk)) \quad \text{and} \quad \tau = \alpha r \mu_0 e^{-\frac{n}{a}r} \tag{16}$$

where

$$I(n) = e^{-n} (n^3 + 3n^2 + 6n + 6) \tag{17}$$

And, Eq. (16) resulted in:

$$\tau = \frac{n^4 T}{2\pi a^4 (I(n) - I(nk))} r e^{-\frac{n}{a}r} \tag{18}$$

2.3. Analysis of other FGM models

Another verification attempt was made regarding the FGM cylinder with Poisson's ratio and Young's modulus varying as (Model C):

$$\begin{aligned} \nu &= \nu_c V_c + \nu_m (1 - V_c) \\ E &= E_c V_c + E_m (1 - V_c) \end{aligned} \tag{19}$$

This model was taken from [24]. The region between the inner and outer surfaces was made of the combined ceramic-metal material with different mixing ratios of ceramic and metal in which indices of c and m implied ceramic and metal, respectively. The volume fraction of the ceramic constituent was defined as:

$$V_c = \left(\frac{r-a}{b-a}\right)^n \tag{20}$$

An additional model (Model D) expressed for metal-ceramic FGM was given in [25]. Overall, Poisson's ratio and modulus of elasticity were assumed to vary as:

$$E = E_c \frac{2\left(1 + \frac{\beta r}{a}\right) - (1 - \nu_c) e^{\frac{\gamma r}{a}}}{(1 + \nu_c) \left(1 + \frac{\beta r}{a}\right)^2} \quad \text{and} \quad \mu = \frac{\mu_c}{1 + \frac{\beta r}{a}} \tag{21}$$

$$\nu = 1 - \frac{(1 - \nu_c) e^{\frac{\gamma r}{a}}}{1 + \frac{\beta r}{a}}$$

where the constants β and γ were given by

$$\begin{aligned} \beta &= \frac{\mu_c}{\mu_m} - 1 \\ \gamma &= \ln(1 + \beta) + \ln \frac{1 - \nu_m}{1 - \nu_c} \end{aligned} \tag{22}$$

In Eq. (22), E_c, ν_c and μ_c are Young's modulus, Poisson's ratio and the shear modulus

of the ceramic constituent and E_m, ν_m, μ_m are those of the metal constituent.

Firstly, the material properties given by these models were substituted in Eq. (10). Then, using Eqs. (2) and (3), the torque of twist and the shear stress were subsequently calculated. These terms would yield extremely complex expressions; that is why, they were not explicitly given in the present paper.

3. Finite element analysis

A specimen was modeled using a commercial FE code, ABAQUS. An “8-node linear brick” element was used to represent the FGM specimen. The analysis of problem would have to take a long time because of modeling the specimen in three-dimensional space. For the sake of overcoming this problem, the cylinder could be modeled as a short length cylinder (disk) instead of long cylinder. Actually, by the symmetry of the problem, it was reasonable to assume that the motion of each cross-sectional plane induced by the end moments was a rigid body rotation about the z-axis. The final FEM model consisted of 28000 elements in total. In the model, the variation in material properties was implemented by dividing the thickness to 10 layers with each layer having a constant value of the material properties [26, 27]. For applying the torsional load, one side of the cylinder was tied by a circular rigid plane and the torque was exerted in the center of circular rigid plane. Besides, the circular plane was free to rotate about z-axis while constraining the other directions alone. Another side of the cylinder was fixed completely. The characteristics of the model are listed in Table 1. Figure 2 shows the meshing region and the element type.

Table 1. Characteristics of the finite element model.

Characteristics of the model	
Cylinder length (m)	$l=0.005$
Inner radius (m)	$a=0.04$
Outer radius (m)	$b=0.06$
Exerted torque (kN.m)	$T=1$

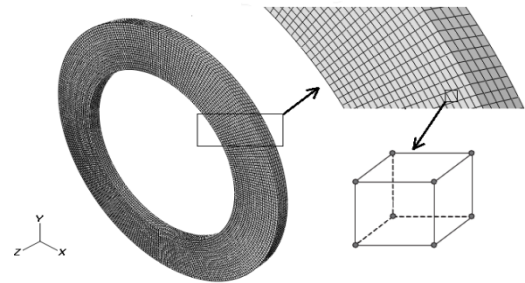


Fig. 2. Finite element mesh region and element type.

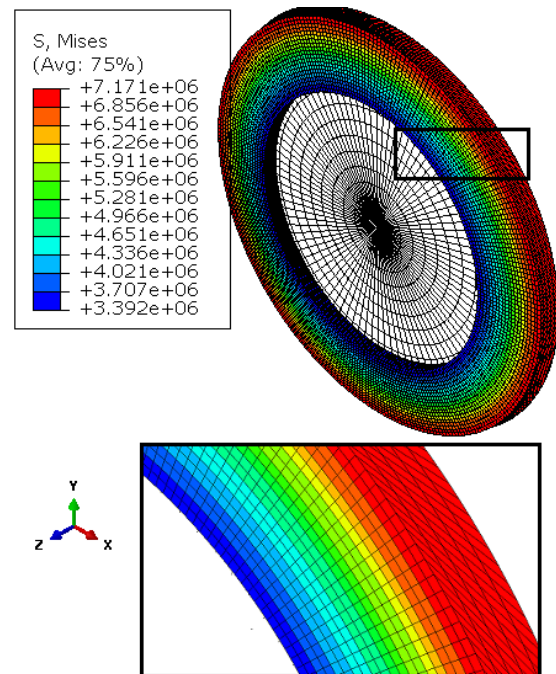


Fig. 3. Deformed shape and von Mises stress distributions for model (A) for $n = 1$.

4. Results and discussion

The analytical solution and FE analysis presented in the previous section were applied to a thick hollow cylinder with the characteristics listed in Table 1.

First, using the properties $E_0 = 200(GPa)$ and $\nu = 0.3$, the Models A and B were examined.

Figure 3 illustrates the deformed shape and von Mises stress distributions at the cross section of cylinder for model (A) for $n = 1$.

Results of the presented formulation and FEM solutions are compared in Figs. 4 to 11.

4.1 Model (A)

Figure 4 demonstrates shear stress for different values of n through thickness in that the results were normalized with respect to the homogenous cylinder results, being explored for the effect of inhomogeneity.

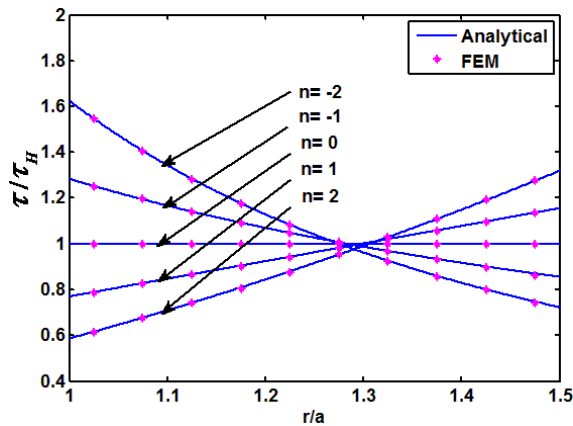


Fig. 4. Distribution of dimensionless shear stress with respect to r/a for different values of n (MODEL A).

According to the Fig. 4, the dimensionless shear stress increased from inner to outer surface for $n > 0$ whereas it reduced for $n < 0$. Approximately for $r/a = 1.27$, stress values for all values of n converged toward the stress values in the homogenous material ($n = 0$).

Distribution of shear stress with respect to its values at the inner surface is plotted in Fig. 5.

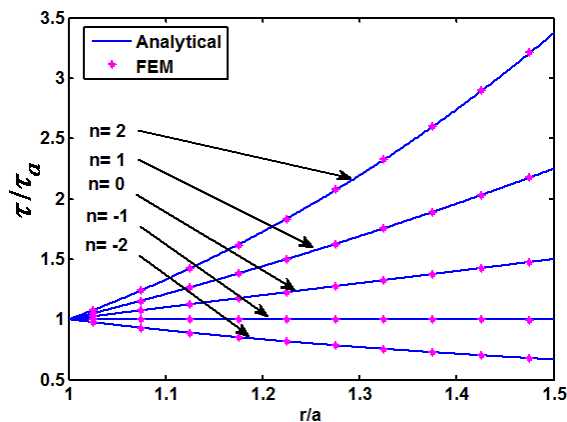


Fig. 5. Distribution of normalized shear stress with respect to inner values (Model A).

Looking at the Fig. 5, it can be said that there was a growth for $n > -1$ from inner to outer surface. But, for $n < -1$, the situation was reversed and the shear stress decreased along the radial direction. The curve associated with $n = -1$ showed that the shear stress remained unchanged along the radial direction which could provide a useful trend from a design point of view. Regarding Eq. (14), the shear stress value throughout thickness could be obtained

$$\text{as: } \frac{3T}{2\pi a^3 (k^3 - 1)}$$

stress variation was linear with respect to the thickness for isotropic cylinder (Fig. 5).

The angle of twist per unit length in terms of n is shown in Fig. 6. Here, a higher value of n meant increasing of the stiffness (See Eq. (11)). It was observed that the angle of twist declined as inhomogeneity constant increased.

4.2 Model (B)

For model B, Fig.7 illustrates the dimensionless shear stress for different values of n through thickness. In the Fig. 7, the distribution of shear stress is plotted regarding the homogenous state.

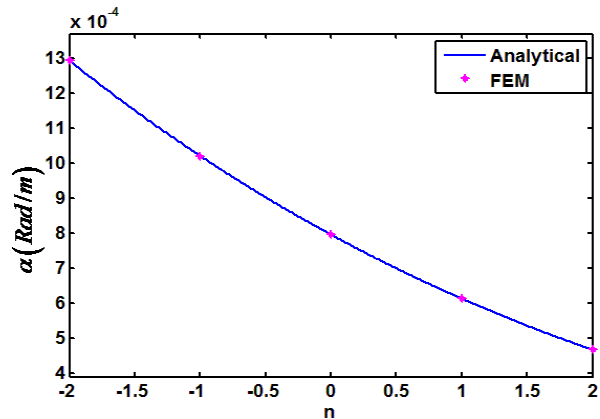


Fig. 6. Variation of the angle of twist per unit length in terms of the power law index (Model A).

For positive values of n , larger stress values were observed at the inner surface of the cylinder and they decreased along the radius. For the negative values of n , smaller stress values were obtained at the inner surface with respect to homogenous cylinder.

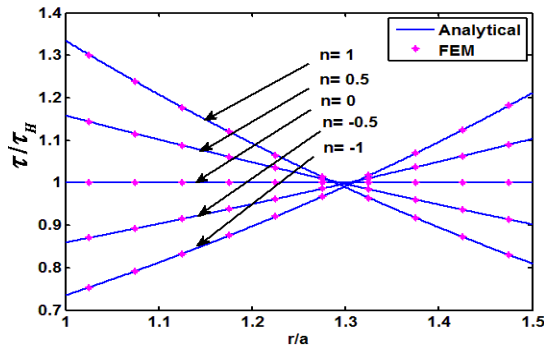


Fig. 7. Distribution of normalized shear stress with respect to homogenous cylinder (Model B).

Here again, an approximate radial distance was $r = 1.27$ and the stress values for all values of n converged towards the stress values in the homogenous material ($n = 0$).

For studying variation along thickness, the distribution of shear stress with respect to values at the inner surface can be seen from the Fig. 8. Given this information, it can be pointed out that the rate of the shear stress variations decreased along the radial direction for higher values of n and, for $n = 0$, these variations became linear. So, lower values of n gave higher stresses at the outer surface. The curve associated with the minimum variation of the shear stress along the radial direction could be obtained from Eq. (21) for $n = 0.811$.

Actually, in this situation, the trend rose from inner surface to middle of the thickness and reached the peak of its value in the middle layer, which was followed by a decrease from middle layer to the outer surface. It should be emphasized that the shear stress had the same value at the inner and outer surfaces for $n = 0.811$. Hence, the shear stress distribution decreased along the radial direction for $n > 0.811$, while it increased along the radial direction for $n < 0.811$.

The angle of twist versus variations of n is displayed in Fig. 9. At a glance, it can be seen that, for higher n values, the angle of twist increased.

4.3. Metal–ceramic FGM models

For metal–ceramic FGM models (Models C and D), the applied properties were

$$E_c = 360(GPa), \nu_c = 0.333,$$

$$\mu_c = 75(GPa), E_m = 200(GPa), \nu_m = 0.2,$$

$$\mu_m = 150(GPa)$$

Using Maple 11, distribution of shear stress was obtained for metal–ceramic FGM models (Models C and D). Graph of shear stress variation which was normalized with respect to the homogenous cylinder versus radius is plotted in Fig. 10 for different values of n .

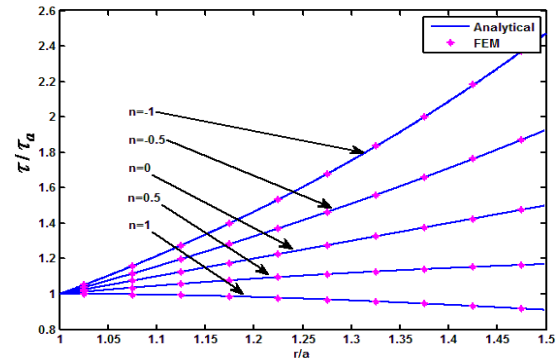


Fig. 8. Distribution of normalized shear stress with respect to inner values (Model B).

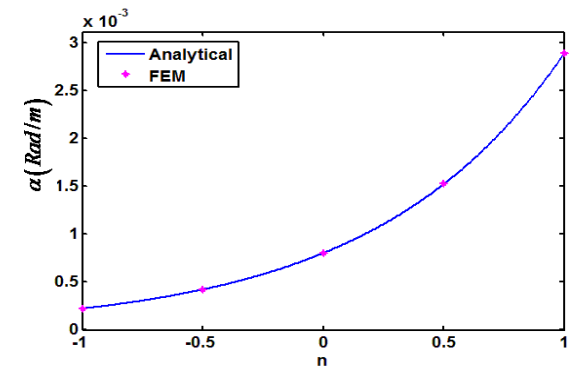


Fig. 9. Variation of the angle of twist versus variation of the power law index (Model B).

Here, $n = 0$ means cylinder material is pure ceramic. As seen, for higher values of n , the shear stress in the regions which were near the inner surface became smoother since these regions were rich of ceramic. In fact, for higher values of n , the proportion of ceramic, rather than metal, increased. So, to put it another way, for the higher values of n , the shear stress distribution near the inner surface tended to become more similar with the pure ceramic one ($n=0$).

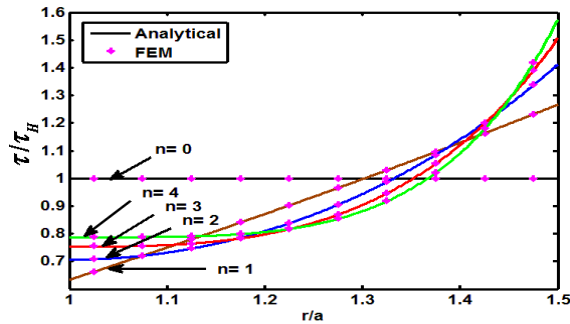


Fig. 10. Distribution of normalized shear stress with respect to homogenous cylinder (Model C).

4. 4. Comparison models

Figure 11 indicates comparison of different models (A through D) for the distribution of shear stress. The typical in homogeneity constant (n) was taken $n = 1$.

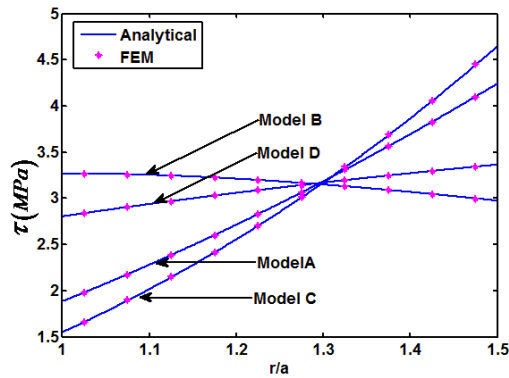


Fig. 11. Comparison of different models (A through D) for the distribution of shear stress for $n = 1$.

Different models resulted in substantial differences in the shear stress distribution through the thickness. For $n = 1$, Models A and C yielded more variation of shear stress than Models B and D. It was also observed that shear stress values converged by about the same magnitude at around $r = 1.29$.

4. 5. Numerical analysis

The numerical analysis was performed with the ABAQUS finite element (FE) package. As seen in the Figs. 4 trough 11, values of the results computed by the present formulation were near the solutions of FEM. Tables 2 and 3 compare the analytical and FEM values determined for different values of r for typical $n = 1$. In fact,

these tables are numerical results of Fig. 11. The percentage of difference was defined as

$$Diff (\%) = \left| \frac{Anal - FEM}{Anal} \right| * 100$$

Considering Tables 2 and 3, it is clear that the $Diff (\%)$ was less than 0.1%. Actually, one can expect that for smaller divisions (more than ten layers), this difference had more decrease.

Table 2. Comparison of analytical and FEM calculations for typical $n = 1$ (for Models A and B).

r/a	Type	MODEL(A)		MODEL(B)	
		Shear stress (Pa)	%Diff	Shear stress (Pa)	%Diff
1.025	Anal.	1981186.8	0.0612	3267151.5	0.0153
	FEM	1982400.0		3266650.0	
1.075	Anal.	2179187.6	0.0605	3259411.2	0.0160
	FEM	2180505.0		3258890.0	
1.125	Anal.	2386617.0	0.0600	3244654.7	0.0163
	FEM	2388050.0		3244125.0	
1.175	Anal.	2603475.0	0.0597	3223584.8	0.0167
	FEM	2605030.0		3223045.0	
1.225	Anal.	2829761.7	0.0593	3196852.5	0.0171
	FEM	2831440.0		3196305.0	
1.275	Anal.	3065476.9	0.0591	3165060.2	0.0174
	FEM	3067290.0		3164510.0	
1.325	Anal.	3310620.8	0.0589	3128765.0	0.0176
	FEM	3312570.0		3128215.0	
1.375	Anal.	3565193.3	0.0585	3088481.7	0.0179
	FEM	3567280.0		3087930.0	
1.425	Anal.	3829194.4	0.0584	3044685.8	0.0179
	FEM	3831430.0		3044140.0	
1.475	Anal.	4102624.1	0.0588	2997815.6	0.0177
	FEM	4105035.0		2997285.0	

Table 3. Comparison of analytical and FEM calculations for typical $n = 1$ (for Models C and D).

r/a	Type	MODEL(C)		MODEL(D)	
		Shear Stress (Pa)	%Diff	Shear Stress (Pa)	%Diff
1.025	Anal.	1661028.2	0.0916	2838067.6	0.0063
	FEM	1662550.0		2838245.0	
1.075	Anal.	1895060.9	0.0910	2904786.8	0.0058
	FEM	1896785.0		2904955.0	
1.125	Anal.	2146603.8	0.0907	2968366.3	0.0052
	FEM	2148550.0		2968520.0	
1.175	Anal.	2416200.0	0.0900	3029022.5	0.0045
	FEM	2418375.0		3029160.0	
1.225	Anal.	2704415.2	0.0897	3086952.7	0.0041
	FEM	2706840.0		3087080.0	
1.275	Anal.	3011839.2	0.0893	3142336.4	0.0041
	FEM	3014530.0		3142465.0	
1.325	Anal.	3339086.8	0.0892	3195338.1	0.0037
	FEM	3342065.0		3195455.0	
1.375	Anal.	3686799.4	0.0888	3246108.1	0.0038
	FEM	3690075.0		3246230.0	
1.425	Anal.	4055646.2	0.0889	3294784.5	0.0037
	FEM	4059250.0		3294905.0	
1.475	Anal.	4446326.2	0.0891	3341494.2	0.0035
	FEM	4450290.0		3341610.0	

5. Conclusions

An exact analytical closed-form formulation was presented for shear stress and angle of twist of hollow cylinder. Material properties of functionally graded material were assumed to be an arbitrary function of radial direction. Several models were served as benchmarks to prove the ability of analytical closed-form. Moreover, the problem was also investigated by finite element method. The comparison between analytical and FEM simulations indicated that the errors were less than 0.1% for the studied cases.

From the above results, it could be seen that the inhomogeneity coefficient “ n ” had a significant effect on the shear stress distribution for different models. Thus, the inhomogeneity constant of FGM cylinder was a useful parameter from a design point of view and could be applied for specific applications to control stress distributions. Finally, an optimum value could be found for n such that variation of stresses along the radial direction was minimized. Hence, in this paper, for model (A) in which material properties change as the power law function, the curve associated with $n = -1$ the shear stress along the radial direction was constant. And for model (B) in which the material properties changed as the exponential law function, the curve related to $n = 0.811$ nearly resulted in a uniform shear stress distribution with the same values at the inner and outer surfaces and a peak value at the middle layer.

References

- [1] S. P. Timoshenko and J. N. Goodier, *Theory of Elasticity*, McGraw-Hill, New York, (1970).
- [2] F. M. Baron, “Torsion of Multi-Connected Thin-Walled Cylinders”, *J. Appl. Mech.*, Vol. 9, pp. 72-74, (1942).
- [3] Z. Li, J. M. Ko and Y. Q. Ni, “Torsional Rigidity of Reinforced Concrete Bars with Arbitrary Sectional Shape”, *Finite Elem. Anal. Des.*, Vol. 35, pp. 349-361, (2000).
- [4] G. Mejak, “Optimization of cross-section of hollow prismatic bars in torsion”, *Communications in Numerical Methods in Engineering*, Vol. 16, pp. 687-695, (2000).
- [5] W. G. Jiang and J. L. Henshall, “A coupling cross-section finite element model for torsion analysis of prismatic bars”, *Eur. J. Mech. A/Solids*, Vol. 21, pp. 513-522, (2002).
- [6] M. Louis Angelo and M. Ryan, “Torsion of a rectangular prismatic bar: Solution using a power fit model”, *Philippine Engineering Journal*, Vol. 28, No. 1, pp. 77-98, (2007).
- [7] A. Doostfatemeh, M. R. Hematiyan and S. Arghavan, “Closed-form approximate formulations for torsional analyses of hollow tube with straight and circular edges”, *Journal of Mechanics*, Vol. 25, pp. 401-409, (2009).
- [8] M. Koizumi, “The concept of FGM”. *Composites Part B*, Vol. 28(B), pp. 1-4, (1993).
- [9] S. Suresh and A. Mortensen, *Fundamentals of functionally graded materials*, Cambridge Publication, London, (1998).
- [10] C. O. Horgan and A. M. Chan, “The pressurized hollow cylinder or disk problem for functionally graded isotropic linearly elastic materials”. *J. Elasticity*, Vol. 55, No. 1, pp. 43-59, (1999).
- [11] M. K. Kassir, “Boussinesq problems for a nonhomogeneous solid”, *J. Engng. Mech.*, Vol. 98, pp. 457-470, (1972).
- [12] M. K. Kassir and M. F. Chauprasert, “A rigid punch in contact with a non-homogeneous solid”, *J. Appl. Mech.*, Vol. 42, pp. 1019-1024, (1974).
- [13] N. Tutuncu, “Stresses in thick-walled FGM cylinders with exponentially-varying properties”, *Eng. Struct.* Vol. 29, pp. 2032-35, (2007).
- [14] C. O. Horgan and A. M. Chan, “Torsion of functionally graded isotropic linearly elastic bars”, *J. Elasticity*, Vol. 52, pp. 181-199, (1999).
- [15] S. A. Moeini and M. T. Ahmadian, “Structural Analysis of Stiffened FGM Thick Walled Cylinders by Application of a New Cylindrical Super Element”, *World Academy of Science, Engineering and Technology*, Vol. 58, pp. 116-121, (2009).

- [16] S. Arghavan and M. R. Hematiyan, "Torsion of functionally graded hollow tubes", *European Journal of Mechanics A/Solids*, Vol. 28, pp. 551-559, (2009).
- [17] I. Ecsedi, "A formula for the generalized twist", *Int. J. Solids Struct.*, Vol. 41, pp. 4097-4105, (2004).
- [18] R. C. Batra, "Torsion of a functionally graded cylinder", *AIAA J.*, Vol. 44, pp. 1363-1365, (2006).
- [19] N. Tutuncu and B. Temel, "A novel approach to stress analysis of pressurized FGM cylinders, disks and spheres", *Composite Structures*, Vol. 91, pp. 385-390, (2009).
- [20] X. F. Li and X. L. Peng, "A Pressurized Functionally Graded Hollow Cylinder with Arbitrarily Varying Material Properties", *J. Elast*, Vol. 96, pp. 81-95, (2009).
- [21] X. L. Peng and X. F. Li, "Thermoelastic analysis of a cylinder vessel of functionally graded materials", *International journal of pressure vessels and piping*, Vol. 87, pp. 203-210, (2010).
- [22] G. J. Nie, Z. Zhong and R. C. Batra, "Material tailoring for orthotropic elastic rotating disks", *Composites Science and Technology*, Vol. 71, pp. 406-14, (2011).
- [23] H. Sadd, *Elasticity theory, applications, and numerics*, 2^{ed} ed., Burlington, MA01803, USA, (2009).
- [24] K. M. Liew, X. Q. He, T. Y. Ng and S. Kitipornchai, "Finite element piezothermoelasticity analysis and the active control of FGM plates with integrated piezoelectric sensors and actuators", *Comput. Mech.*, Vol. 31, pp. 350-58, (2003).
- [25] Z. H. Jin and R. C. Batra, "Some basic fracture mechanics concepts in functionally graded materials", *J. Mech. Phys. Solids*, Vol. 44, pp. 1221-1235, (1996).
- [26] K. S. Ravi and I. Barsoum, "Determination of stress intensity factor solutions for cracks in finite-width functionally graded materials", *International Journal of Fracture*, Vol. 121, pp. 183-203, (2003).
- [27] Y. Bayat, M. Ghannad and H. Torabi, "Analytical and Numerical Analysis for the FGM Thick Sphere under Combined Pressure and Temperature Loading", *Arch. Appl. Mech.*, Vol. 82, pp. 229-242, (2012).